

Gamma-delayed deuteron emission of the ${}^6\text{Li}(0^+; T = 1)$ halo state

E.M. Tursunov ^{a,b}, P. Descouvemont ^{a,1}, and D. Baye ^{c,a}

^a*Physique Nucléaire Théorique et Physique Mathématique, C.P. 229, Université Libre de Bruxelles, B1050 Brussels, Belgium*

^b*Institute of Nuclear Physics, Uzbekistan Academy of Sciences, 702132, Ulugbek, Tashkent, Uzbekistan*

^c*Physique Quantique, C.P. 165/82, Université Libre de Bruxelles, B1050 Brussels, Belgium*

Abstract

M1 transitions from the ${}^6\text{Li}(0^+; T = 1)$ state at 3.563 MeV to the ${}^6\text{Li}(1^+)$ ground state and to the $\alpha + d$ continuum are studied in a three-body model. The bound states are described as an $\alpha + n + p$ system in hyperspherical coordinates on a Lagrange mesh. The ground-state magnetic moment and the gamma width of the ${}^6\text{Li}(0^+)$ resonance are well reproduced. The halo-like structure of the ${}^6\text{Li}(0^+)$ resonance is confirmed and is probed by the M1 transition probability to the $\alpha + d$ continuum. The spectrum is sensitive to the description of the $\alpha + d$ phase shifts. The corresponding gamma width is around 1.0 meV, with optimal potentials. Charge symmetry is analyzed through a comparison with the β -delayed deuteron spectrum of ${}^6\text{He}$. In ${}^6\text{He}$, a nearly perfect cancellation effect between short-range and halo contributions was found. A similar analysis for the ${}^6\text{Li}(0^+; T = 1)$ γ decay is performed; it shows that charge-symmetry breaking at large distances, due to the different binding energies and to different charges, reduces this effect. The present branching ratio $\Gamma_\gamma(0^+ \rightarrow \alpha + d)/\Gamma_\gamma(0^+ \rightarrow 1^+) \approx 1.3 \times 10^{-4}$ should be observable with current experimental facilities.

Key words: ${}^6\text{Li}$, gamma decay, charge symmetry

PACS: 23.40.Hc, 21.45.+v, 21.60.Gx, 27.20.+n

Email addresses: tursune@inp.uz (E.M. Tursunov), pdesc@ulb.ac.be (P. Descouvemont), dbaye@ulb.ac.be (D. Baye).

¹ Directeur de Recherches FNRS

1 Introduction

Electromagnetic transition processes provide a useful tool for the study of the nuclear structure and of the reaction mechanisms. The theoretical study of such processes yields estimates for the different static and dynamical observables of a nucleus. In ${}^6\text{Li}$, the $(0^+; T = 1)$ state has raised interest as a good candidate for observing parity violation [1,2]. Indeed, its decay into the $\alpha + d$ continuum is forbidden by parity conservation. Since electromagnetic M1 transitions into this continuum are allowed, they have been also studied because they may compete with the parity-violating decay and make its detection difficult.

However, the ${}^6\text{Li}(0^+; T = 1)$ state is also interesting by itself. It is most likely a halo state, as it is the isobaric analog of the ${}^6\text{He}$ ground state [3]. M1 transitions to the continuum are in fact also an excellent tool to explore these halo properties and compare them with those of ${}^6\text{He}$. Recent experimental and theoretical works on the delayed ${}^6\text{He}$ β decay suggest that the deuteron spectrum is strongly sensitive to the halo structure (see Ref. [4] and references therein). Similarities between this process and the γ -delayed deuteron emission of ${}^6\text{Li}(0^+)$ are expected, and should test charge symmetry in exotic light nuclei.

The branching ratio of the total transition probability to the $\alpha + d$ continuum and the transition probability to the ${}^6\text{Li}(1^+)$ ground state was estimated as 8×10^{-5} under a number of simplifying assumptions [2]. However the shape and magnitude of the transition probability to the continuum as a function of the deuteron energy were not studied. In addition, the sensitivity with respect to the $\alpha + d$ potential, as well as convergence problems, were not addressed. The aim of the present work is to investigate M1 transitions from the ${}^6\text{Li}(0^+)$ excited state to the $\alpha + d$ continuum, as well as to the ${}^6\text{Li}(1^+)$ ground state. For the description of the ${}^6\text{Li}$ states, we use different two-body and three-body models. Three-body hyperspherical wave functions [5] are based on the Lagrange-mesh method and give an accurate solution of the three-body Schrödinger equation [6]. The $\alpha + d$ scattering wave function is factorized into a deuteron wave function and a nucleus-nucleus scattering state. This work extends our previous study on ${}^6\text{He}$ β decay where the same formalism was used.

The model is presented in Section 2. The potentials and the corresponding two-body and three-body wave functions are also described. In Section 3, we discuss the results in comparison with the experimental data, and analyze the sensitivity with respect to the $\alpha + d$ potential. Finally, conclusions are given in Section 4.

2 Model

2.1 Three-body wave functions of ${}^6\text{Li}$ bound states

The ${}^6\text{Li}$ bound-state wave functions are defined in an $\alpha + n + p$ model using the hyperspherical coordinates [5]. A set of Jacobi coordinates for three particles with mass numbers $A_1 = 1$, $A_2 = 1$, and $A_3 = 4$ is defined as

$$\mathbf{x} = \sqrt{\mu_{pn}} \mathbf{r}, \quad \mathbf{y} = \sqrt{\mu_{\alpha d}} \mathbf{R}, \quad (1)$$

where the (dimensionless) reduced masses are given by $\mu_{pn} = 1/2$ and $\mu_{\alpha d} = 4/3$. The $p - n$ relative coordinate and the coordinate between α and d are denoted by \mathbf{r} and \mathbf{R} , respectively. Equations (1) define six coordinates which are transformed to the hyperspherical coordinates as

$$\rho^2 = x^2 + y^2, \quad \alpha = \arctan(y/x), \quad (2)$$

where α varies between 0 and $\pi/2$. With the angular variables $\Omega_x = (\theta_x, \varphi_x)$ and $\Omega_y = (\theta_y, \varphi_y)$, equations (2) define a set of hyperspherical coordinates which are known to be well adapted to the three-body Schrödinger equation.

We define $\gamma = (\ell_x, \ell_y, L, S)$ where ℓ_x and ℓ_y are the orbital momenta associated with the Jacobi coordinates \mathbf{x} and \mathbf{y} , respectively. With the notation $\Omega_5 = (\alpha, \Omega_x, \Omega_y)$, a three-body wave function with spin J and parity π reads [6]

$$\Psi_{{}^6\text{Li}}^{JM\pi}(\rho, \Omega_5) = \rho^{-5/2} \sum_{\gamma K} \chi_{\gamma K}^{J\pi}(\rho) \mathcal{Y}_{\gamma K}^{JM}(\Omega_5), \quad (3)$$

where $\mathcal{Y}_{\gamma K}^{JM}(\Omega_5)$ are the hyperspherical functions (including spin), defined as

$$\begin{aligned} \mathcal{Y}_{\gamma K}^{JM}(\Omega_5) &= \phi_K^{\ell_x \ell_y}(\alpha) \left[[Y_{\ell_x}(\Omega_x) \otimes Y_{\ell_y}(\Omega_y)]^L \otimes \chi^S \right]^{JM}, \\ \phi_K^{\ell_x \ell_y}(\alpha) &= \mathcal{N}_K^{\ell_x \ell_y} (\cos \alpha)^{\ell_x} (\sin \alpha)^{\ell_y} P_n^{\ell_y + \frac{1}{2}, \ell_x + \frac{1}{2}}(\cos 2\alpha), \end{aligned} \quad (4)$$

with $n = (K - \ell_x - \ell_y)/2$, and where $\mathcal{N}_K^{\ell_x \ell_y}$ is a normalization factor, $P_n^{a,b}$ a Jacobi polynomial and χ^S a spin function. Details are given in Refs. [5,6]. The hyperradial functions $\chi_{\gamma K}^{J\pi}$ are obtained from a set of coupled equations truncated at $K = K_{max}$. The problem is solved by using the Lagrange-mesh technique (see Ref. [6] for details).

The three-body wave functions contain components with total intrinsic spin

$S = 0$ and $S = 1$. Because of the positive parity, $\ell_x + \ell_y$ is even and only even K values are involved.

2.2 $\alpha + d$ two-body wave functions

As it was done in Ref. [4] for the ${}^6\text{He}$ β decay, the scattering $\alpha + d$ wave functions are factorized into a deuteron ground-state wave function, calculated with an appropriate NN potential, and an $\alpha + d$ wave function derived from a potential model. We neglect the small D component of the deuteron. In the $\alpha + d$ exit channel, only S waves are involved. Consequently, the final 1^+ wave function reads

$$\Psi_{\alpha d}^{1M+}(E, \mathbf{r}, \mathbf{R}) = \Psi_d(\mathbf{r}) \Psi_{\alpha d}(E; \mathbf{R}). \quad (5)$$

The spatial part of the deuteron wave function is written as

$$\Psi_d(\mathbf{r}) = r^{-1} u_d(r) Y_{00}(\hat{\mathbf{r}}). \quad (6)$$

The S -wave component of the $\alpha + d$ relative motion wave function is factorized as

$$\Psi_{\alpha d}(E; \mathbf{R}) = R^{-1} u_E(R) Y_{00}(\hat{\mathbf{R}}). \quad (7)$$

The normalization of the scattering wave function is fixed by the asymptotic behaviour as

$$u_E(R) \xrightarrow{R \rightarrow \infty} F_0(k_{\alpha d} R) \cos \delta_0(E) + G_0(k_{\alpha d} R) \sin \delta_0(E), \quad (8)$$

where F_0 and G_0 are the Coulomb functions, $\delta_0(E)$ is the s -wave phase shift at energy E , and $k_{\alpha d}$ is the wave number of the relative motion.

The present two-body model can also be applied to $\alpha + d$ bound states. In that case, the scattering wave function $u_E(R)$ in Eq. (7) is replaced by an S -wave bound-state radial function.

2.3 Transition probability per time and energy units

For the M1 transition to the ground state, the gamma width is calculated from

$$\Gamma_\gamma(0^+ \rightarrow 1^+) = \frac{16\pi}{9} k_\gamma^3 |\langle \Psi_{6\text{Li}}^{1+} || \mathcal{M}_1^M || \Psi_{6\text{Li}}^{0+} \rangle|^2, \quad (9)$$

where k_γ is the wave number of the emitted photon. This definition involves bound-state wave functions on both sides.

With the normalization (8) of the scattering wave function, the M1 transition probability of the process

$${}^6\text{Li}(0^+) \rightarrow \alpha + d + \gamma, \quad (10)$$

per time and energy units, is given by reduced matrix elements between the initial bound state and the final scattering states as (see Appendix A)

$$\frac{dW_\gamma}{dE} = \frac{32\mu_{ad}m_N}{3\hbar^3 k_{\alpha d}} k_\gamma^3 |\langle \Psi_{\alpha d}^{1+}(E) || \mathcal{M}_1^M || \Psi_{6\text{Li}}^{0+} \rangle|^2, \quad (11)$$

where m_N is the nucleon mass. The maximum $\alpha + d$ energy is $Q = 2.089$ MeV. The M1 differential gamma width per energy unit to continuum states is expressed as

$$\frac{d\Gamma_\gamma(0^+ \rightarrow \alpha + d)}{dE} = \hbar \frac{dW_\gamma}{dE}, \quad (12)$$

and the total width is deduced by integration over the energy.

The M1 operator contains orbital and spin-dependent components. For a general three-body system, it reads, in Jacobi coordinates [6]

$$\begin{aligned} \mathcal{M}_{1\mu}^M(\mathbf{x}, \mathbf{y}) = \mu_N \sqrt{\frac{3}{4\pi}} [& A_x \ell_{x,\mu} + A_y \ell_{y,\mu} + A_{xy} (\mathbf{x} \times \mathbf{p}_y + \mathbf{y} \times \mathbf{p}_x)_\mu \\ & + \sum_{i=1}^3 g_s(i) \mathbf{s}_{i\mu}], \end{aligned} \quad (13)$$

where $\mu_N = e\hbar/m_N c$ is the nuclear magneton, \mathbf{s}_i are the spins of the three particles, and $g_s(i)$ their gyromagnetic factors. Coefficients A_x , A_y and A_{xy} are related to the mass and charge numbers as

$$\begin{aligned}
A_x &= \frac{Z_2 A_1^2 + Z_1 A_2^2}{A_1 A_2 A_{12}}, \\
A_y &= \frac{(Z_1 + Z_2) A_3^2 + Z_3 A_{12}^2}{A A_{12} A_3}, \\
A_{xy} &= \sqrt{\frac{A_1 A_2 A_3}{A_{12}^2 A}} \left(\frac{Z_1}{A_1} - \frac{Z_2}{A_2} \right),
\end{aligned} \tag{14}$$

where A_{12} is the reduced mass of the $1 + 2$ system; in the present case it is denoted as μ_{pn} . Variables \mathbf{p}_x and \mathbf{p}_y are the momenta associated with the Jacobi coordinates \mathbf{x} and \mathbf{y} , respectively. The matrix elements of the M1 operator between hyperspherical functions are given in Appendix B.

3 Results and discussion

3.1 Conditions of the calculations

3.1.1 Three-body wave functions of the 1^+ and 0^+ states

The initial 0^+ wave function is calculated in an $\alpha + n + p$ three-cluster model, using hyperspherical coordinates, as explained in Ref. [6]. The same model is applied to the ${}^6\text{Li}$ ground state. In both cases, the Coulomb $\alpha + p$ interaction is included, and is taken as a point-sphere potential parameterized as $V_C(r) = 2e^2 \text{erf}(r/R_C)$ with a radius $R_C = 1.2$ fm. Two-body forbidden states are removed by using the Orthogonalising Pseudopotential method [7]. The central Minnesota interaction [8] describes the $n + p$ system. It is adjusted on the deuteron binding energy and reproduces fairly well nucleon-nucleon phase shifts at low energies. For the $\alpha + N$ nuclear interaction we employ the potential of Voronchev *et al.* [9], slightly renormalized by a scaling factor (1.008 for 1^+ and 1.043 for 0^+) to reproduce the experimental energies with respect to the three-body threshold (-3.70 MeV for the ground state, and -0.13 MeV for the 0^+ state). We truncate the hypermomentum expansion to $K_{max} = 20$ which ensures a good convergence of the energies.

The matter r.m.s. radius of the ground state (with 1.4 fm as α radius) is found as $\sqrt{\langle r^2 \rangle} = 2.25$ fm, a value slightly lower than the experimental value (2.32 ± 0.03 fm [10]) (note however that a significantly larger radius, 2.54 ± 0.03 fm, was found in Ref. [11]). For the excited 0^+ level, we find $\sqrt{\langle r^2 \rangle} = 2.56$ fm, which is close to the ${}^6\text{He}$ radius. This large value confirms the halo structure of this state [12]. The ground state is essentially $S = 1$ (96.0%). The $S = 0$ component is 84.4% for ${}^6\text{Li}(0^+)$ and 82.1% for ${}^6\text{He}$. The ${}^6\text{Li}(0^+)$ and ${}^6\text{He}$ hyperradial wave functions are plotted in Fig. 1 for the dominant $K = 0, 2$ hypermomenta. The overlap $\langle {}^6\text{He} | T^+ / \sqrt{2} | {}^6\text{Li}(0^+) \rangle = 0.996$

is in good agreement with the value of Arai *et al* [12] (0.995). According to charge symmetry the short-range parts of the ${}^6\text{He}$ and ${}^6\text{Li}(0^+)$ analog levels should be very close to each other. This is confirmed by Fig. 1. On the contrary, the halo components of both wave functions are expected to differ significantly: the charges of the halo nucleons are different, and the binding energy of ${}^6\text{Li}(0^+)$ is much lower. Consequently, the asymptotic decrease of the wave function is slower, and matrix elements involving this long-range part should be different from their analogs in ${}^6\text{He}$.

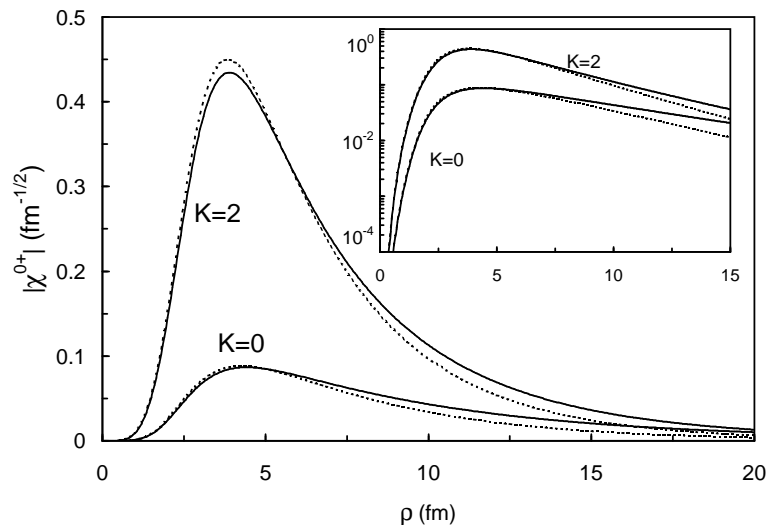


Fig. 1. Hyperradial wave functions for ${}^6\text{Li}(0^+)$ (solid lines) and ${}^6\text{He}$ (dashed lines) corresponding to $S = L = 0, K = 0, 2$. The insert shows the same plot in a logarithmic scale.

3.1.2 $\alpha + d$ scattering states

In the following we use four different $\alpha + d$ potentials (the phase shifts can be found in Ref. [4]):

- (1) The attractive Gaussian potential of Ref. [13] V_a contains a forbidden state and provides the correct ${}^6\text{Li}$ binding energy ($E_1 = -1.473$ MeV, with respect to the $\alpha + d$ threshold). Owing to the presence of a forbidden state, it also provides a good fit of the low-energy experimental phase shifts.
- (2) To test the influence of the short-range part of the $\alpha + d$ wave functions, and in particular of the node location, we also use the potential V_a^{S1} , obtained from a supersymmetric transformation [14]. The resulting potential gives the same phase shifts and the same ground-state energy as the initial potential, but the forbidden state is removed and the role of the Pauli principle is simulated by a short-range core.
- (3) The calculation is complemented by two folding potentials, using the deuteron wave function Ψ_d provided by the Minnesota potential. These

potentials present one forbidden state. The folding potential V_{f1} is obtained from the original $\alpha + N$ potential with a renormalization factor 1.068, which yields the correct binding energy for ${}^6\text{Li}$; however the quality of the S -wave phase shift is poor. The folding potential V_{f2} with a renormalization factor 1.15 describes the S -wave phase shift accurately, but overestimates the binding energy of the ${}^6\text{Li}$ ground state (-2.386 MeV).

In all cases, the $\alpha + d$ Coulomb potential is chosen as in Ref. [13], i.e. as a bare Coulomb potential.

3.2 M1 properties of bound states

A test of three-body wave functions is provided by M1 spectroscopic properties, which are well known experimentally [15]. In Table 1, we present the calculated values of the magnetic moment and of the $B(M1)$ in ${}^6\text{Li}$. Separate contributions are given for the orbital and spin terms of the M1 operator [see Eq. (13)]. In both cases, the contribution of the orbital term is small since the dominant component in the ground-state wave function is an S wave. The main contribution to the M1 matrix element comes from the spin term. The present matrix element corresponds to $B(M1) = 7.9$ W.u., or $\Gamma_\gamma = 7.5$ eV, which are in good agreement with experiment (8.62 ± 0.18 W.u. and 8.19 ± 0.17 eV, respectively). The results are also close to those of Kukulin *et al.* [16] who use different variants of a three-body model.

Table 1

Contributions (in μ_N) of the orbital (L) and spin (S) components to the M1 matrix elements. The three-body model is used for the 0^+ state. Experimental data are taken from [15].

	(L)	(S)	Sum	Exp.
<hr/> <u>Three-body model for 1^+</u>				
$\mu({}^6\text{Li})$	0.02	0.84	0.86	0.82
$\langle \Psi_{6\text{Li}}^{1+} \mathcal{M}_1^M \Psi_{6\text{Li}}^{0+} \rangle$	0.13	2.04	2.17	2.28
<hr/> <u>Two-body model for 1^+</u>				
$\mu({}^6\text{Li})$	0	0.88	0.88	0.82
$\langle \Psi_{6\text{Li}}^{1+} \mathcal{M}_1^M \Psi_{6\text{Li}}^{0+} \rangle$	0.04	1.53	1.57	2.28

These matrix elements can also be obtained with a 2-body description of the ${}^6\text{Li}$ ground state. In that case we use the potential V_a to generate the wave

functions. Since components with $L \neq 0$ are small in the ground-state wave function, the two-body model is expected to be a good approximation. The 1^+ magnetic moment in the two-body model is a simple sum of the proton and neutron magnetic moments. In this case, both approaches provide similar results, in good agreement with experiment. However the rms radius in the two-body model is $\sqrt{\langle r^2 \rangle} = 2.11$ fm, lower than experiment and than the three-body value (see Sect.3.1.1). In addition, the M1 transition matrix element (see Table 1) provides $\Gamma_\gamma = 3.9$ eV, i.e. an underestimate of the experimental value. These results suggest that the short-range part of the two-body description is too simple. However, transitions to the continuum are more sensitive to the long-range part of the $\alpha - d$ wave functions.

3.3 M1-transition to the $\alpha + d$ continuum: effective wave functions and their integrals

Since the $\alpha + d$ relative motion is described by S waves, the first and second orbital terms of the M1 transition operator (13) do not contribute to the reduced matrix elements for transitions to the $\alpha + d$ continuum. The orbital and spin terms yield nonzero matrix elements only for the $\ell_x = \ell_y = L = S = 1$ and $\ell_x = \ell_y = L = S = 0$ components of the three-body wave function, respectively. As it will be shown further, the main contribution comes from the spin part of the transition operator. The P -wave hyperspherical components give small corrections to the process since the 0^+ state is essentially $S = 0$.

In order to analyze the γ -decay process to the continuum, we introduce effective wave functions and their integrals, in analogy with the β -decay study of the ${}^6\text{He}$ halo nucleus into the $\alpha + d$ continuum [4]. We restrict the presentation to the dominant spin part. For the initial 0^+ state, let us define the effective wave function with hypermomentum K

$$u_{\text{eff}}^{(K)}(R) = \left(\frac{A-2}{A}\right)^{3/4} R \int dr \phi_K^{00}(\alpha) \frac{\chi_{0000K}^{0+}(\rho)}{\rho^{5/2}} r u_d(r), \quad (15)$$

and the effective integrals

$$\begin{aligned} I_E^{(K)}(R) &= \int_0^R dR' u_E(R') u_{\text{eff}}^{(K)}(R'), \\ I_E(R) &= \sum_K I_E^{(K)}(R), \end{aligned} \quad (16)$$

where ρ and α depend on (r, R) , as given in Eq. (2). The normalization factor in Eq. (15) arises from the Jacobian between the (\mathbf{R}, \mathbf{r}) and (\mathbf{x}, \mathbf{y}) coordinates.

The reduced matrix elements of the M1 operator (spin part) are then directly proportional to $I_E(R)$ (see Appendix B).

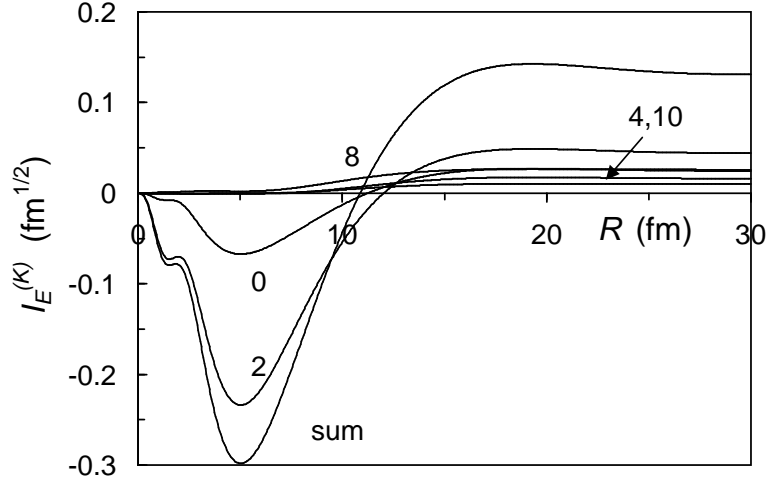


Fig. 2. Integrals $I_E^{(K)}(R)$ [Eq.(16)] at $E = 1$ MeV for the $\alpha + d$ potential V_a and different K values (labels).

In the following, we analyze two properties: the convergence of the hypermomentum expansion, and the sensitivity of the effective integrals with respect to the $\alpha + d$ potential. Let us start with the influence of K_{\max} . In Fig. 2 we show the integrals $I_E^{(K)}(R)$ calculated at $E = 1$ MeV with potential V_a , for different K -values. The dominant contribution at large R values comes from the $K = 0, 2, 8$ components in the ${}^6\text{Li}(0^+)$ wave function. The components $K = 4$ and $K = 10$ give smaller and comparable effects to the process. The contributions of other components are small and not visible at the scale of the figure. Similar results were obtained for the β decay of ${}^6\text{He}$ [4]. In Ref. [4] it was shown that the $K = 4$ and $K = 6$ contributions are affected by cancellation effects, which do not occur for $K \geq 8$. The situation is therefore very close to the ${}^6\text{He}(0^+)$ beta decay [4] into the $\alpha + d$ continuum which confirms the halo structure of the ${}^6\text{Li}(0^+)$ state, suggested by its large r.m.s. radius.

In the second step, we analyze the sensitivity of the effective integrals with respect to the potential. In Fig. 3, these integrals are shown at $E = 1$ MeV. The potentials V_a and V_{f2} , which provide similar phase shifts and wave functions, give results close to each other. This is due to the similar node positions near 5 fm of the corresponding scattering wave functions. The folding potential V_{f1} , owing to a poor phase-shift description, yields a scattering wave function with an inner node shifted to the right (about 0.7 fm), and therefore provides a different integral.

In Fig. 3, we also show as dotted lines, for each potential, the effective integrals obtained for the ${}^6\text{He}$ β decay [4] (notice that in Ref. [4], the factor $((A - 2)/A)^{3/4} = 0.74$ in the effective wave function was missing). In that work, we have shown that a node in the $\alpha + d$ continuum wave functions is

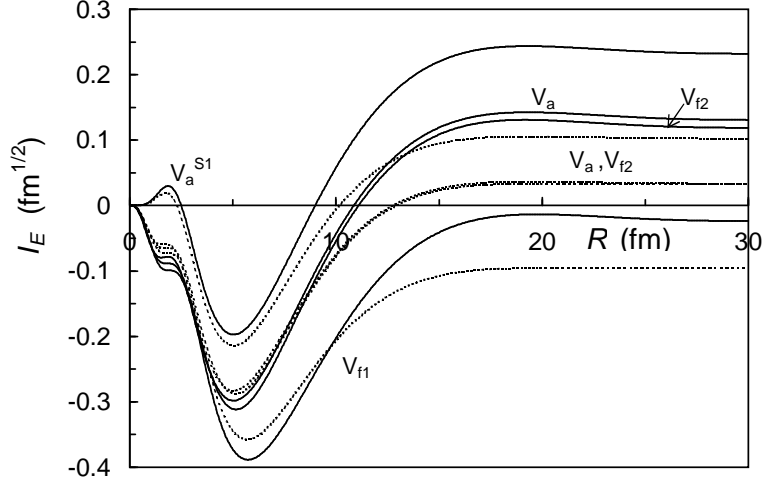


Fig. 3. Effective integrals $I_E(R)$ [Eq.(16)] at $E = 1$ MeV for different $\alpha + d$ potentials (solid lines). Dotted lines represent the equivalent integrals for the ${}^6\text{He}$ β decay [4].

responsible for a nearly perfect cancellation effect in the β -decay matrix element. This is illustrated in Fig. 3: for the recommended potential V_a , the internal contribution to the matrix element is about -0.30 whereas the external term is about $+0.35$. The final result is therefore much lower than each component individually. This phenomenon yields a strong sensitivity of the β spectrum with respect to the $\alpha + d$ potential.

Coming back to the γ decay of the ${}^6\text{Li}$ analog level (solid lines in Fig. 3), the internal parts of the matrix elements are very close to their ${}^6\text{He}$ counterparts up to about 10 fm. However, as the long-range parts of the wave functions are different in both nuclei, the external contribution to the γ -decay matrix element is significantly larger (about $+0.42$ for V_a). Consequently, a cancellation effect still occurs, but is less important. If we disregard potential V_{f1} which does not reproduce the $\alpha + d$ phase shifts, and hence the correct location of the nodes in the continuum wave functions, all potentials provide the same sign for the matrix element.

3.4 $M1$ -transitions to the $\alpha + d$ continuum: transition probabilities

In Table 2 we give the contributions of different K values to the M1 reduced matrix element into the $\alpha + d$ continuum. As we noted above, the orbital and spin parts of the M1 transition operator yield nonzero matrix elements only with the $\ell_x = \ell_y = L = S = 1$ (P -wave) and $\ell_x = \ell_y = L = S = 0$ (S -wave) components of the three-body wave function, respectively. As expected from the previous analysis, the dominant contributions come from the $K = 0, 2$ and 8 components. Additionally, the contribution of the orbital part of the

M1 transition operator is strongly suppressed (2% at most).

Table 2

Contribution of different ${}^6\text{Li}(0^+)$ hypermomenta to the M1 reduced matrix elements for transitions into the $\alpha + d$ continuum (in $10^{-3}\mu_N$) for the orbital (L) and spin (S) terms at several energies

	$E = 0.5 \text{ MeV}$		$E = 1 \text{ MeV}$		$E = 1.5 \text{ MeV}$	
K	(L)	(S)	(L)	(S)	(L)	(S)
0	0	-56.9	0	-54.2	0	-46.4
2	0.5	-85.9	0.6	-104.9	0.4	-115.6
4	3.1	-36.3	4.5	-31.0	5.2	-21.0
6	1.5	-11.4	2.1	-4.9	2.2	1.4
8	-1.2	-51.1	-1.6	-61.6	-1.7	-61.3
10	-0.3	-22.2	-0.3	-23.1	-0.3	-20.0
> 10	0.3	-21.2	0.4	-14.5	0.4	-7.3
Sum	3.9	-285.0	5.7	-294.2	6.2	-270.2

To analyze the convergence with respect to the upper bound R_{max} [see Eq. (16)], we display in Fig. 4 the differential width $d\Gamma_\gamma/dE$ for several values of R_{max} (potential V_a is used). From Fig. 4, one can see that $R_{\text{max}} = 10 \text{ fm}$ is far from sufficient. Achieving a precise convergence requires larger values ($\sim 25 - 30 \text{ fm}$), as in the beta-decay calculations of the ${}^6\text{He}$ halo nucleus into the $\alpha + d$ continuum [4]. This is not surprising as the halo structure of ${}^6\text{Li}(0^+)$ is even more pronounced (see Fig. 1).

In Fig. 5, we display the differential width $d\Gamma_\gamma/dE$ for several $\alpha + d$ potentials. Contributions from three-body components up to $K_{\text{max}} = 20$ are taken into account with the maximal relative distance $R_{\text{max}} = 30 \text{ fm}$. The folding potential V_{f1} shows a picture strongly different from the other ones, with even a sharp minimum at about $E = 0.8 \text{ MeV}$. This potential gives a poor description of the $\alpha + d$ phase shift (see Ref. [4]) and hence a shifted node position for the $\alpha + d$ scattering wave function. This results in a strong cancellation effect as explained in the previous section. The folding potential V_{f2} and the deep potential V_a give close results and the supersymmetric potential V_a^{S1} slightly overestimates them.

The integrated γ widths (from $E = 0$ up to $Q = 2.089 \text{ MeV}$) are given in Table 3 for the different potentials. The Gaussian potential V_a simultaneously reproduces both the ${}^6\text{Li}$ ground state binding energy and the S -wave phase shift at low energies. Additionally, the S -wave scattering wave function of this

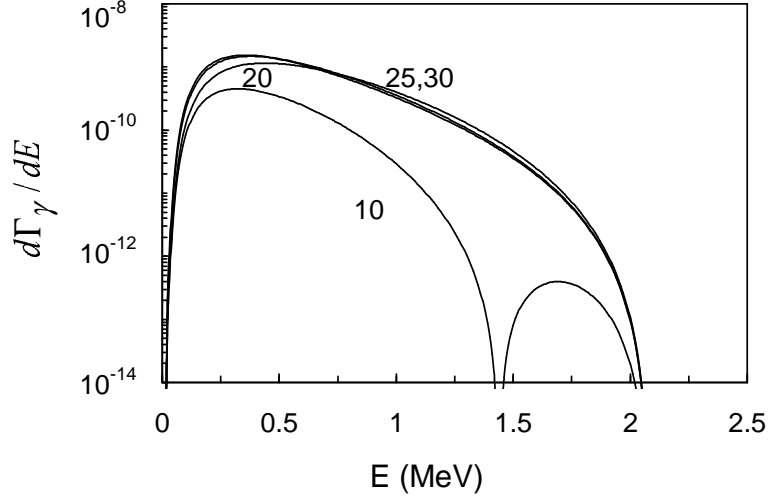


Fig. 4. Differential width for M1 transitions into the $\alpha + d$ continuum with the $\alpha + d$ potential V_a for several values of R_{\max} (in fm).

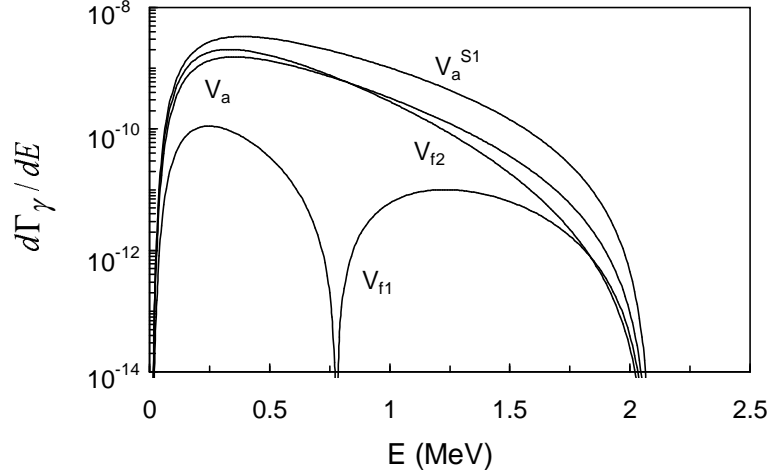


Fig. 5. Differential width for M1 transitions into the $\alpha + d$ continuum for several potentials.

potential has two nodes at short distances (one due to the ground state, and one due to the Pauli forbidden state). The nearly phase-equivalent potential V_{f2} , which also has a forbidden bound state (and hence two nodes at short distances) gives similar results.

The influence of the nodes in the scattering wave function can be tested by using potential V_a^{S1} . The non-physical ground state of V_a is removed by using a supersymmetric transformation [14]. The resulting phase-equivalent potential V_a^{S1} has exactly the same ${}^6\text{Li}$ ground-state energy and the same S -wave phase shift as V_a but its scattering wave functions have one node less at small distances. The corresponding width of the M1 transition is about two times larger (see Table 3). In the ${}^6\text{He}$ β -decay process, this potential strongly overestimates the data [4]. Notice that a very different result is obtained with the

folding potential V_{f1} , which has two bound states, but does not reproduce the $\alpha + d$ phase shifts and the ${}^6\text{He}$ delayed β decay. The shape and magnitude of the transition width and probability are strongly different from the result for V_a .

Table 3

Integrated γ widths for different potentials, and branching ratio $BR = \Gamma_\gamma(0^+ \rightarrow \alpha + d)/\Gamma_\gamma(0^+ \rightarrow 1^+)$ (we use the theoretical value $\Gamma_\gamma(0^+ \rightarrow 1^+) = 7.5 \text{ eV}$).

potential	Γ_γ (meV)	BR
V_a	0.90	1.2×10^{-4}
V_{f1}	0.04	5.3×10^{-6}
V_{f2}	1.08	1.4×10^{-4}
V_a^{S1}	2.27	3.0×10^{-4}

Considering the V_a and V_{f2} potentials, which are consistent with the data on ${}^6\text{He}$ β decay, we deduce a recommended branching ratio of 1.3×10^{-4} by averaging both values. A previous estimate [2] of the branching ratio $\Gamma_\gamma(0^+ \rightarrow \alpha + d)/\Gamma_\gamma(0^+ \rightarrow 1^+)$ provides 0.8×10^{-4} . This value is close to our results obtained with potential V_a [13], and is also similar to the branching ratio observed in the β decay of ${}^6\text{He}$ [17]. Such a branching ratio should be observable experimentally.

4 Conclusions

In the present work, we have studied the M1 transition process from the ${}^6\text{Li}(0^+)$ halo state into the $\alpha + d$ continuum and into the ${}^6\text{Li}(1^+)$ ground state. Our goal was twofold: (i) to determine the energy distribution of the γ width for the decay into the continuum, and to analyze its sensitivity with respect to the $\alpha + d$ potential; (ii) to compare this process with the ${}^6\text{He}$ β -delayed decay. This comparison is a good tool to test charge symmetry in exotic nuclei. The ${}^6\text{Li}(0^+, 1^+)$ states are defined in the three-body hyperspherical formalism. The experimental magnetic moment of the ground state and γ width of the $0^+, T = 1$ state are reproduced with a good accuracy.

We have shown that the spin-dependent term of the M1 transition operator gives the essential part of the matrix elements. In order to test the influence of the ${}^6\text{Li}$ bound-state wave functions, we have also used the supersymmetric transform [14] instead of the Orthogonalising Pseudopotential method for the

removal of forbidden states in the three-body wave functions. The results are very similar to the present ones, and were therefore not shown.

In the M1 transition probability, the $K = 0$ and $K = 2$ components of the three-body wave function provide about 50% of the matrix elements; consequently, higher hypermomenta play an important role. The same conclusion holds in the ${}^6\text{He}$ β decay into the $\alpha + d$ continuum, where large K values cannot be neglected.

M1 transitions to the continuum provide a good probe of the halo structure in the ${}^6\text{Li}(0^+)$ state. The comparison with the ${}^6\text{He}$ β decay shows that the inner parts of the matrix elements are very close to each other, as expected from charge symmetry. However, the halo parts are different, owing to the different binding energies, and different charges of the halo nucleons. In ${}^6\text{Li}$, the binding energy is lower, and therefore the asymptotic decrease of the wave function is slower. Consequently the halo contribution is larger in the γ -decay matrix element, and even represents the dominant part. This leads to the conclusion that charge-symmetry breaking is rather strong in these processes. The nearly perfect cancellation effect between short-range and halo contributions observed in ${}^6\text{He}$ β -decay is less important here, and the sensitivity with respect to the potential is therefore weaker. Several $\alpha + d$ potentials were tested. The sensitivity is still important (about a factor of 2), but lower than in the ${}^6\text{He}$ β -delayed decay.

The present branching ratio of about 1.3×10^{-4} is consistent with the value of Ref. [2], where the authors use a simplified model. The present value is based on potential V_a which reproduces the ${}^6\text{Li}$ binding energy, the $\alpha + d$ low-energy phase shifts, and provides fair results for the ${}^6\text{He}$ β decay. It is therefore expected to have the same quality for the ${}^6\text{Li}$ γ decay. An experimental measurement seems to be possible with current facilities, and would provide, in combination with the data on ${}^6\text{He}$ β decay, an important step in a better understanding of the halo structure in isobaric analog states.

Acknowledgements

This text presents research results of the Belgian program P5/07 on interuniversity attraction poles initiated by the Belgian-state Federal Services for Scientific, Technical and Cultural Affairs (FSTC). E.M.T. acknowledges the support of the National Fund for Scientific Research (FNRS), Belgium. E.M.T. thanks the PNTPM group of ULB for its kind hospitality during his stay in Brussels.

A Gamma delayed transition probabilities to continuum states

Let us assume a bound initial state at energy E_i with spin and parity J_i, π_i of a nucleus at rest, decaying to a final unbound state at relative energy E , and with spin and parity J_f, π_f . In the final state, both nuclei are characterized by spins I_1 and I_2 , and by internal wave functions ϕ^{I_1} and ϕ^{I_2} . According to Ref. [18], the transition probability per time unit is given by

$$dW_\gamma = \frac{2\pi}{\hbar} \frac{|T_{fi}|^2}{(2\pi\hbar)^6} d\mathbf{p} d\mathbf{P} d\mathbf{p}_\gamma \delta(\mathbf{P} + \mathbf{p}_\gamma) \delta(E + E_\gamma - E_i), \quad (\text{A.1})$$

where we neglect recoil effects. In (A.1), $(\mathbf{p}, \mathbf{P}, \mathbf{p}_\gamma)$ are the relative, total, and photon momenta. The transition matrix element T_{fi} is obtained from

$$|T_{fi}|^2 = \frac{1}{2J_i + 1} \frac{2\pi\hbar c}{k_\gamma} \sum_{\nu_1, \nu_2, M_i, q} |\langle \Psi_f^{\nu_1\nu_2(-)}(\mathbf{p}) | H_\gamma^q | \Psi^{J_i M_i \pi_i} \rangle|^2, \quad (\text{A.2})$$

where (ν_1, ν_2) are the spin orientations in the exit channel, H_γ^q is the electromagnetic-emission hamiltonian with polarization q , and k_γ is the photon wave number. The final state is described by an ingoing wave $\Psi_f^{\nu_1\nu_2(-)}$ with relative momentum $\mathbf{p} = (p, \Omega_p)$, related to the corresponding outgoing wave $\Psi_f^{\nu_1\nu_2(+)}$ by

$$\Psi_f^{\nu_1\nu_2(-)}(\mathbf{p}) = (-1)^{I_1+I_2-\nu_1-\nu_2} K \Psi_f^{-\nu_1-\nu_2(+)}(-\mathbf{p}), \quad (\text{A.3})$$

where K is the time-reversal operator. The outgoing wave function is written in a partial wave expansion as

$$\Psi_f^{\nu_1\nu_2(+)}(\mathbf{p}) = \sum_{JM\pi\ell I\nu} \langle I_1 I_2 \nu_1 \nu_2 | I \nu \rangle \langle \ell I m \nu | J M \rangle \Psi_{\ell I}^{JM\pi}(E) \mathcal{D}_{0m}^{\ell*}(\Omega_p), \quad (\text{A.4})$$

where $\mathcal{D}_{0m}^\ell(\Omega_p)$ are Wigner functions. When the relative coordinate \mathbf{r} is large, the asymptotic behaviour of the partial wave is given by

$$\begin{aligned} \Psi_{\ell I}^{JM\pi}(E) \longrightarrow & \frac{[\pi(2\ell+1)]^{1/2}}{kr} i^{\ell+1} \exp(i\sigma_\ell) \left(I_\ell(kr) - U^{J\pi} O_\ell(kr) \right) \\ & \times [[\phi^{I_1} \otimes \phi^{I_2}]^I \otimes Y_\ell(\Omega_r)]^{JM}, \end{aligned} \quad (\text{A.5})$$

where σ_ℓ are the Coulomb phase shifts, and I_ℓ and O_ℓ are the ingoing and outgoing Coulomb functions, respectively. Here and in the following, we assume a

single-channel problem or, in other words, that the dimension of the collision matrix \mathbf{U} is unity.

After integration over \mathbf{P} and p_γ , Eq. (A.1) is transformed as

$$dW_\gamma = \frac{k_\gamma^2}{(2\pi\hbar)^5 c} |T_{fi}|^2 d\mathbf{p} d\Omega_\gamma. \quad (\text{A.6})$$

First, we expand H_γ^q in electric ($\sigma = E$) and magnetic ($\sigma = M$) multipoles [19]. Then we integrate over the orientations Ω_p and Ω_γ . We have

$$\begin{aligned} \int |T_{fi}|^2 d\Omega_p d\Omega_\gamma &= \frac{32\pi^2}{2J_i + 1} \sum_{\sigma\lambda J_f \pi_f} \frac{|\alpha_\lambda^\sigma|^2}{2\lambda + 1} \\ &\times \frac{2J_f + 1}{2\ell_f + 1} |\langle \Psi_{\ell_f I_f}^{J_f \pi_f}(E) | | \mathcal{M}_\lambda^\sigma | | \Psi^{J_i \pi_i} \rangle|^2, \end{aligned} \quad (\text{A.7})$$

where $\mathcal{M}_\lambda^\sigma$ are the multipole operators of order λ (coefficients α_λ^σ are given, for instance, in Ref. [19]). Let us define

$$\Gamma_\gamma(E) = \sum_{\sigma\lambda J_f \pi_f} \frac{8\pi k_\gamma^{2\lambda+1}}{\lambda(2\lambda+1)!!^2} \frac{2J_f + 1}{2J_i + 1} |\langle \Psi_{\ell_f I_f}^{J_f \pi_f}(E) | | \mathcal{M}_\lambda^\sigma | | \Psi^{J_i \pi_i} \rangle|^2. \quad (\text{A.8})$$

Using (A.7) in (A.6) gives

$$\frac{dW_\gamma}{dE} = \frac{\mu k}{2\pi^2 \hbar^3} \frac{\Gamma_\gamma(E)}{2\ell_f + 1}, \quad (\text{A.9})$$

where μ is the reduced mass. An interesting case concerns transitions to a narrow resonance with energy E_R and particle width Γ . In such a case, the scattering wave function can be approximated as [20]

$$\Psi_{I_f \ell_f}^{J_f \pi_f}(E) \approx \frac{1}{k} \frac{[\pi \hbar v (2\ell_f + 1) \Gamma]^{1/2}}{E_R - E - i\Gamma/2} \Psi_{BSA}^{J_f \pi_f}, \quad (\text{A.10})$$

where $\Psi_{BSA}^{J_f \pi_f}$ is the bound-state approximation of the wave function, and v the relative velocity. Using this approximation in (A.9) and integrating over E gives

$$W_\gamma = \Gamma_\gamma^{BSA} / \hbar, \quad (\text{A.11})$$

where Γ_γ^{BSA} is the γ width in the bound-state approximation. This result corresponds to the usual definition of the transition probability between two bound states.

B Matrix elements of the M1 transition operator in hyperspherical coordinates

Let us write the three-body wave function (3) as

$$\Psi_{\delta\text{Li}}^{JM\pi}(\rho, \Omega_5) = \rho^{-5/2} \sum_{\gamma K} \chi_{\gamma K}^{J\pi}(\rho) \mathcal{Y}_{\gamma K}^{JM}(\Omega_5) = \sum_{\gamma K} \Psi_{\gamma K}^{JM\pi}(\rho, \Omega_5), \quad (\text{B.1})$$

where index γ stands for $(\ell_x \ell_y LS)$. A reduced matrix element of ℓ_x is obtained from

$$\begin{aligned} \langle \Psi_{\gamma K}^{J\pi} || \ell_x || \Psi_{\gamma' K'}^{J'\pi'} \rangle &= \delta_{\ell_x \ell'_x} \delta_{\ell_y \ell'_y} \delta_{SS'} \delta_{KK'} [\ell_x (\ell_x + 1)]^{1/2} \hat{\ell}_x \hat{L} \hat{L}' \hat{J}' \\ &\times (-)^{\ell_x + \ell_y + S + L + L' + J'} \begin{Bmatrix} L & \ell_x & \ell_y \\ \ell_x & L' & 1 \end{Bmatrix} \begin{Bmatrix} L & J & S \\ J' & L' & 1 \end{Bmatrix} I_\rho, \end{aligned} \quad (\text{B.2})$$

where we use the notation $\hat{\ell} = \sqrt{2\ell + 1}$, and where the integral I_ρ is defined as

$$I_\rho = \int \chi_{\gamma K}^{J\pi}(\rho) \chi_{\gamma' K'}^{J'\pi'}(\rho) d\rho. \quad (\text{B.3})$$

Matrix elements of ℓ_y are obtained by swapping ℓ_x and ℓ_y . For the crossed term in (13), the calculation is more tedious. We have

$$\begin{aligned} \langle \Psi_{\gamma K}^{J\pi} || \mathbf{x} \times \mathbf{p}_y + \mathbf{y} \times \mathbf{p}_x || \Psi_{\gamma' K'}^{J'\pi'} \rangle &= \delta_{SS'} (-)^{L+S+J'+\ell_x+\ell_y} \sqrt{6} \hat{\ell}_x \hat{\ell}_y \hat{\ell}'_x \hat{\ell}'_y \hat{L} \hat{L}' \hat{J}' \\ &\times \begin{pmatrix} \ell'_x & 1 & \ell_x \\ 0 & 0 & 0 \end{pmatrix} \begin{pmatrix} \ell'_y & 1 & \ell_y \\ 0 & 0 & 0 \end{pmatrix} \begin{Bmatrix} L & J & S \\ J' & L' & 1 \end{Bmatrix} \begin{Bmatrix} \ell_x & \ell_y & L \\ \ell'_x & \ell'_y & L' \\ 1 & 1 & 1 \end{Bmatrix} I_\rho I_\alpha, \end{aligned} \quad (\text{B.4})$$

where the angular integral reads

$$I_\alpha = \int_0^{\pi/2} d\alpha \cos^2 \alpha \sin^2 \alpha \phi_K^{\ell_x \ell_y}(\alpha) \left(\frac{d}{d\alpha} + \frac{\Delta \ell_y}{\tan \alpha} - \frac{\Delta \ell_x}{\cot \alpha} \right) \phi_{K'}^{\ell'_x \ell'_y}(\alpha). \quad (\text{B.5})$$

In this expression, $\Delta\ell = 1 + [\ell'(\ell' + 1) - \ell(\ell + 1)]/2$. Integration over α is performed numerically. For the hyperradius ρ , the use of Lagrange functions makes the integral very simple.

For the spin part of the M1 operator, we have

$$\begin{aligned} \langle \Psi_{\gamma K}^{J\pi} || \mathbf{s}_1 || \Psi_{\gamma' K'}^{J'\pi'} \rangle &= \delta_{\ell_x \ell'_x} \delta_{\ell_y \ell'_y} \delta_{LL'} \delta_{KK'} \hat{s}_1 \hat{S} \hat{S}' \hat{J}' [s_1(s_1 + 1)]^{1/2} \\ &\times (-)^{s_1+s_2+L-J} \left\{ \begin{matrix} J & S & L \\ S' & J' & 1 \end{matrix} \right\} \left\{ \begin{matrix} S & s_1 & s_2 \\ s_1 & S' & 1 \end{matrix} \right\} I_\rho, \end{aligned} \quad (\text{B.6})$$

where we have assumed that the core spin is zero ($s_3 = 0$).

For transitions to the continuum, the previous formula can still be applied, but the final-state wave functions are now defined by Eq. (5). It is clear that with the restriction to the S -wave final state, the orbital components $\ell_{x,\mu}$ and $\ell_{y,\mu}$ do not contribute to the M1 transition. The matrix element of the crossed term is performed over the Jacobi coordinates. Using the S -wave character of the scattering state, we have

$$\begin{aligned} \langle \Psi_{6\text{Li}}^{0+} || \mathbf{x} \times \mathbf{p}_y + \mathbf{y} \times \mathbf{p}_x || \Psi_{\alpha d}^{1+} \rangle &= \sqrt{2\mu_{pn}\mu_{\alpha d}/9} \sum_K \int dxdy \phi_K^{11}(\alpha) \chi_{1111K}^{0+}(\rho) \\ &\times xy \rho^{-5/2} \left(x \frac{\partial}{\partial y} - y \frac{\partial}{\partial x} \right) u_d(x/\sqrt{\mu_{pn}}) u_E(y/\sqrt{\mu_{\alpha d}}), \end{aligned} \quad (\text{B.7})$$

where ρ and α are given in Eq. (2). The spin contribution is obtained with the same technique, with the help of Eq. (B.6). Note that the bra and ket have been swapped with respect to Eq. (11). The ordering is simply restored with a factor $-1/\sqrt{3}$.

References

- [1] A. Cs  t  , K. Langanke, Nucl. Phys. A 601 (1996) 131.
- [2] L.V. Grigorenko, N.B. Shulgina, Phys. Atom. Nucl. 61 (1998) 1472.
- [3] Y. Suzuki, K. Yabana, Phys. Lett. B 272 (1991) 173.
- [4] E.M. Tursunov, D. Baye, P. Descouvemont, Phys. Rev. C 73 (2006) 014303; Phys. Rev. C 74 (2006) 069904(E).
- [5] M.V. Zhukov, B.V. Danilin, D.V. Fedorov, J.M. Bang, I.J. Thompson, J.S. Vaagen, Phys. Rep. 231 (1993) 151.

- [6] P. Descouvemont, C. Daniel, D. Baye, Phys. Rev. C 67 (2003) 044309.
- [7] V.I. Kukulin, V.N. Pomerantsev, Ann. Phys. NY 111 (1978) 330.
- [8] D.R. Thompson, M. LeMere, Y.C. Tang, Nucl. Phys. A 286 (1977) 53.
- [9] V.T. Voronchev, V.I. Kukulin, V.N. Pomerantsev, G.G. Ryzhikh, Few-Body Syst. 18 (1995) 191.
- [10] I. Tanihata, T. Kobayashi, O. Yamakawa, S. Shimoura, K. Ekuni, K. Sugimoto, N. Takahashi, T. Shimoda, H. Sato, Phys. Lett. 206B (1988) 592.
- [11] M. Puchalski, A.M. Moro, K. Pachucki, Phys. Rev. Lett. 97 (2006) 133001.
- [12] K. Arai, Y. Suzuki, K. Varga, Phys. Rev. C 51 (1995) 2488.
- [13] S.B. Dubovichenko, A.V. Dzhazairov-Kakhramanov, Phys. Atom. Nucl. 57 (1994) 733.
- [14] D. Baye, Phys. Rev. Lett. 58 (1987) 2738.
- [15] D.R. Tilley, C.M. Cheves, J.L. Godwin, G.M. Hale, H.M. Hofmann, J.H. Kelley, C.G. Sheu, H.R. Weller, Nucl. Phys. A 708 (2002) 3.
- [16] V.I. Kukulin, V.N. Pomerantsev, Kh.D. Razikov, V.T. Voronchev, G.G. Ryzhikh, Nucl. Phys. A 586 (1995) 151.
- [17] D. Anthony, L. Buchmann, P. Bergbusch, J.M. D'Auria, M. Dombisky, U. Giesen, K.P. Jackson, J.D. King, J. Powell, F.C. Barker, Phys. Rev. C 65 (2002) 034310.
- [18] L.S. Rodberg, R.M. Thaler, *Introduction to the quantum theory of scattering*, Academic Press (New York, 1967).
- [19] H.J. Rose, D.M. Brink, Rev. Mod. Phys. 393 (1967) 306.
- [20] D. Baye, P. Descouvemont, Nucl. Phys. A 443 (1985) 302.